
CGB-DM: Content and Graphic Balance Layout Generation with Transformer-based Diffusion Model

Yu Li* Yifan Chen* Gongye Liu Jie Wu Yujiu Yang†

Tsinghua University

<https://yuli0103.github.io/CGB-DM.github.io/>

Abstract

Layout generation is the foundation task of intelligent design, which requires the integration of visual aesthetics and harmonious expression of content delivery. However, existing methods still face challenges in generating precise and visually appealing layouts, including blocking, overlap, or spatial misalignment between layouts, which are closely related to the spatial structure of graphic layouts. We find that these methods overly focus on content information and lack constraints on layout spatial structure, resulting in an imbalance of learning content-aware and graphic-aware features. To tackle this issue, we propose Content and Graphic Balance Layout Generation with Transformer-based Diffusion Model (CGB-DM). Specifically, we first design a regulator that balances the predicted content and graphic weight, overcoming the tendency of paying more attention to the content on canvas. Secondly, we introduce a graphic constraint of saliency bounding box to further enhance the alignment of geometric features between layout representations and images. In addition, we adapt a transformer-based diffusion model as the backbone, whose powerful generation capability ensures the quality in layout generation. Extensive experimental results indicate that our method has achieved state-of-the-art performance in both quantitative and qualitative evaluations. Our model framework can also be expanded to other graphic design fields.

1 Introduction

Layout generation aims to generate an appropriate arrangement of elements, such as logos, text and underlays, where each element is defined by a tuple of attributes of category, position and size. This technique is widely applied in posters [13, 29], documents [27, 30, 46], magazines [24, 42], and user interfaces (UIs) [9, 18]. According to the attention of content, Layout generation can be categorized into two types—content-agnostic and content-aware. The content-agnostic task generates layouts without considering the image conditions. The content-aware layout generation, on the other hand, pays attention to generating a fitting layout that harmonizes with the given background image. This paper focuses on the task of content-aware layout generation. We believe that high-quality layouts not only conform to the layout spatial structure, thus addressing the graphic aspects, but also sufficiently perceive image information, thereby excelling in content.

Earlier deep learning-based solutions to content-aware layout generation have extensively explored task-specific generative modeling methods, mainly with generative adversarial networks (GANs) [17, 41, 45, 47], variational autoencoders (VAE) [4] and transformer-based models [16]. Despite possessing many attractive properties, there exists an inherent balance dilemma between learning content-aware features and graphic-aware features, leading to issues such as blocking, small-sized, overlap and misalignment, as shown in Fig. 1. We analyze that 1) GAN-based and

*Equal contribution.

†Corresponding author.

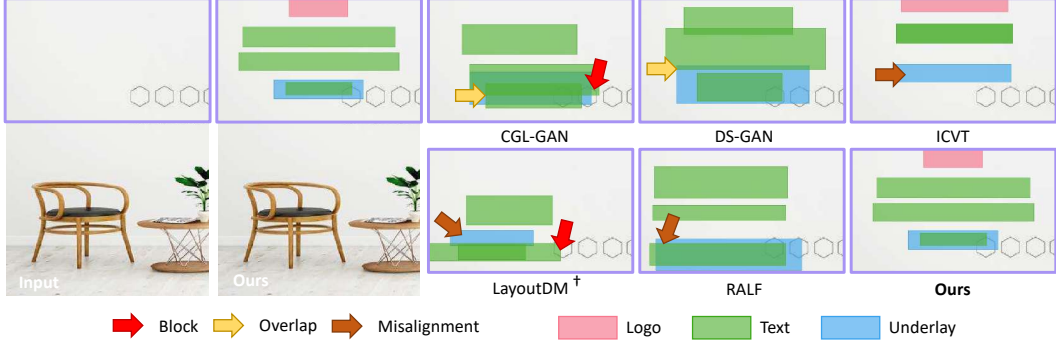


Figure 1: Recent state-of-the-art methods face challenges with blocking, overlap and misalignment, while our method properly improves layout space and presents a coherent arrangement.

Transformer-based methods have limited generative capability in learning layout spatial structure, resulting in poor performance in graphic aspects; 2) current approaches do not effectively balance the focus on content-aware features of images and graphic features of layouts. Consequently, generating high-quality layouts with high quality content and graphics remains a significant challenge.

Recently, generative models [12, 15, 34, 40] have achieved significant advancements, especially as transformer-based diffusion models [3, 7, 11] have emerged as an effective backbone for constructing deep networks. This development hints at the potential for the powerful ability of the generation. To address the above challenges, we propose a method called **Content and Graphic Balance Layout Generation with Transformer-based Diffusion Model (CGB-DM)**. However, the standard transformer-based diffusion, DiT [31] is unsuitable for layout generation. DiT has problems with overlap and misalignment because it cannot process a mixture of geometric and image information. Consequently, we introduce a layout encoder to decouple the learning processes of layouts and images.

We found that issues such as overlapping, misalignment, and blocking arise in current methods. This is because they do not consider the generative space of layouts. In content-agnostic tasks, the generative space of layouts encompasses the entire canvas. While for content-aware tasks, the given background image imposes constraints on the geography of generated layouts, posing challenges to generate content-graphic balanced layouts. These constraints affect the performance of the generated layout in both content and graphic aspects. Therefore, we introduce the content and graphic balance weight to adaptively optimize the generative space for different samples. To further avoid blocking the salient areas in the canvas, we include the saliency bounding box as an additional condition, explicitly extracting the spatial information of the salient areas in the images.

We evaluate the proposed CGB-DM framework on public benchmarks PKU [17] and CGL [47]. The experimental results show that CGB-DM outperforms state-of-the-art models in content-aware layout generation. Notably, our method demonstrates a significant improvement in graphic performance.

Our main contributions can be summarized as follows:

- We are the first to introduce a transformer-based diffusion model to address the challenges in the content-aware layout generation task. Our model framework can also be applied to other graphic design fields or sequence data generation tasks.
- We introduce a content and graphic balance weight to adjust the interaction process between layout representations and image embeddings. We also incorporate a saliency bounding box to enhance the model’s capture of geometric information in images.
- Extensive experimental results show that our method achieves superior performance both quantitatively and qualitatively, significantly outperforming other state-of-the-art methods.

2 Related Work

2.1 Diffusion-based Content-agnostic Layout Generation

Numerous studies on content-agnostic layout generation [1, 14, 20, 37] have incorporated diffusion models into this field. PLay [8] utilizes a conditional latent diffusion model to generate parametrically

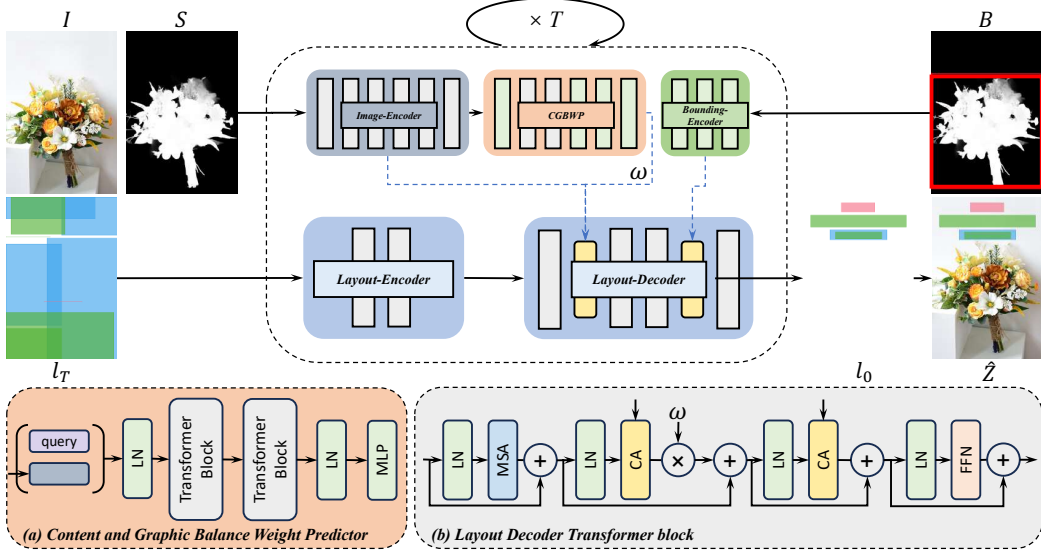


Figure 2: Our framework of Content and Graphic Balance Layout Generation with Transformer-based Diffusion Model (CGB-DM), as well as (a) Content and Graphic Balance Weight Predictor (CGBWP), and the (b) Layout Decoder Transformer block of Layout Decoder.

conditioned layouts in the vector graphic space. LayoutDM [19] and LayoutDiffusion [43] are based on discrete diffusion models [2], treating both geometric parameters and category information as discrete data. Another study [5] employs DDPM to handle geometric parameters in continuous spaces while introducing category information as a condition. In contrast, DLT [25] proposes training discrete and continuous data jointly through a diffusion layout transformer. LACE [6] introduces a unified model that generates in a continuous feature space, enabling the integration of differentiable aesthetic constraint functions during training to guide the optimization of layout generation. Our research aims to expand the generative scope of diffusion models, focusing on exploring how to apply diffusion models to layout generation tasks that include canvas information.

2.2 Content-aware Layout Generation

Content-GAN [45] was the first layout generation model to include both visual and textual content. Subsequently, CGL-GAN [47] focused on addressing the domain misalignment issue, pioneering subsequent research by introducing a saliency map. ICVT [4] differentiated the study of layout elements into the visual domain and geometric parameter domain, proposing a geometry alignment module to align the geometric information of images with layout representations. The DS-GAN [17] team explored the layout generation task using a distinct model architecture CNN-LSTM. RADM [26] was the first to apply the diffusion model to this task. In contrast, our approach utilizes the transformer architecture [38] to model layout elements. RADM developed a visual-textual relation-aware module and a geometry relation-aware module to capture distinct relationships. Finally, RALF [16] approached from a data perspective, identifying that misaligned underlay embellishment and text elements commonly found in prior studies were due to a lack of highly structured layout training data, hence proposing a retrieval-augmented approach to mitigate data scarcity issues.

3 Method

We propose the first effective transformer-based diffusion architecture for layout generation, dubbed **Content and Graphic Balance Layout Generation with Transformer-based Diffusion Model (CGB-DM)**. Fig. 2 shows the overview of our framework. The inputs are Gaussian noise l_T , image I with its saliency map S , and saliency bounding box B . Within the dedicated layout clues, (a) We formulate layout generation into a diffusion model process, gradually denoising to generate coherent and precise layouts; (b) To optimize and balance the generation space of different samples, we introduce the content and graphic balance weight; (c) It's vital to enhance the capability of capturing the geometric

information in images for the model. Therefore, we add a saliency bounding box as an augmentation condition. Our CGB-DM enables the model to simultaneously maintain the effective perception of image content and mastery of layout spatial structure.

3.1 Preliminaries

Saliency map. Let $I \in \mathbb{R}^{H \times W \times 3}$ be the paired canvas and $S \in \mathbb{R}^{H \times W \times 1}$ be its saliency map, where H and W represent the height and width, respectively. We use the off-the-shelf detection method [32, 44] to obtain a saliency map $S \in \mathbb{R}^{H \times W \times 1}$ from the canvas.

Saliency bounding box. Let $B = \{x_s, y_s, w_s, h_s\}$ be the saliency bounding box, where x_s and y_s represent the center coordinates of it, and w_s and h_s indicate its height and weight, respectively. We detect the boundaries of salient areas in the saliency map where pixel values exceed a specific threshold. The saliency bounding area value is expressed as

$$B_{ij} = \begin{cases} 0, & B_{ij} \leq s, \\ 1, & B_{ij} > s, \end{cases} \quad (1)$$

where s is a threshold value and $i = 1, 2, 3, \dots, j = 1, 2, 3, \dots$. Subsequently, we calculate the saliency bounding box based on the minimum rectangle boundaries where $B_{ij} = 1$.

3.2 Transformer-based Layout Diffusion Formulation

Unlike image generation, in the forward and reverse processes of diffusion, we handle data corresponding to layout elements, as illustrated in Fig. 2. Consequently, we consider the layout generation problem as a noise-to-layout generation process conditioned on the image. The layout is defined as a set consisting of N layout elements, denoted as $L = \{l_1, \dots, l_N\} = \{(c_1, b_1), \dots, (c_N, b_N)\}$. In this notation, $c_i \in \{0, 1, \dots, C\}$ represents C categories of layout elements, along with a special category denoted by $c_i = 0$ to signify an empty element. Additionally, $b_i = (x_i, y_i, w_i, h_i) \in [0, 1]^4$ indicates the normalized bounding box.

During the forward diffusion process, we sample L_0 from the true data distribution and gradually add Gaussian noise at each step t :

$$\begin{aligned} q(L_t | L_{t-1}) &= \mathcal{N}(L_t; \sqrt{1 - \beta_t} L_{t-1}, \beta_t \mathbf{I}), \\ q(L_{1:T} | L_0) &= \prod_{t=1}^T q(L_t | L_{t-1}), \end{aligned} \quad (2)$$

where $[\beta_t]_{t=0}^T$ denotes a constant variance schedule that controls the Gaussian noise at each step. We can obtain

$$L_t = \sqrt{\alpha_t} L_0 + \sqrt{1 - \alpha_t} \epsilon, \quad (3)$$

where $\alpha_t = 1 - \beta_t$, $\sqrt{\alpha_t} = \prod_{s=1}^t \alpha_s$, and $\epsilon \sim \mathcal{N}(0, \mathbf{I})$ is the random noise added at time-step t . The reverse process model is trained to invert the forward process by predicting the statistics of p_θ as :

$$p_\theta(L_{t-1} | L_t) = \mathcal{N}(L_{t-1}; \mu_\theta(L_t, t), \Sigma_\theta(L_t, t)). \quad (4)$$

By setting $\Sigma_\theta(L_t, t) = \sigma_t^2 \mathbf{I}$ and reparameterizing μ_θ as a noise predictor network ϵ_θ [15], the model can be easily trained by minimizing the L2 loss between the predicted noise ϵ_θ and the ground truth sampled Gaussian noise ϵ . Specifically, we employ a transformer model to predict the ϵ_θ at each step, the training object can be written as minimizing:

$$\min_{\theta} \mathbb{E}_{L_t, \epsilon \sim \mathcal{N}(0, \mathbf{I}), I, S, B, t} [\|\epsilon - \epsilon_\theta(L_t, I, S, B, t)\|^2]. \quad (5)$$

After ϵ_θ is trained to converge, we can generate desired layouts by initializing $L_T \sim \mathcal{N}(0, \mathbf{I})$ and sampling $L_{t-1} \sim p_\theta(L_{t-1} | L_t)$ gradually until obtain L_0 .

We utilize the layout encoder and decoder as the main backbone. Both of them consist of a series of transformer blocks, as detailed in Fig. 2. Self-attention modules are employed to model the relationships between layout elements, while cross-attention modules facilitate the perceptual interaction of layout representation with the image embedding and saliency bounding box. This iterative denoising and refining process enables us to generate more reasonable and high-quality layouts, especially showing significant improvements in addressing underlay misalignment and text overlap issues.

3.3 Content and Graphic Balance Weight Predictor

In previous work, we have two observations: (1) model often generates small-sized bounding boxes as shown in Fig. 4; (2) the layout elements overlap with the text or logo box and misalign between text and underlay, as illustrated in Fig. 1, affecting the quality and harmony of the layout. In content-agnostic generation tasks [21–23], such unreasonable layouts are typically not produced because the model does not need to consider aligning with the images. Therefore, the generative space is the entire canvas. However, in content-aware tasks, the model tends to avoid blocking the layout with objects of the image, thereby compressing the generative space. We hypothesize that this leads to the phenomenon of overlap, misalignment and small-sized elements.

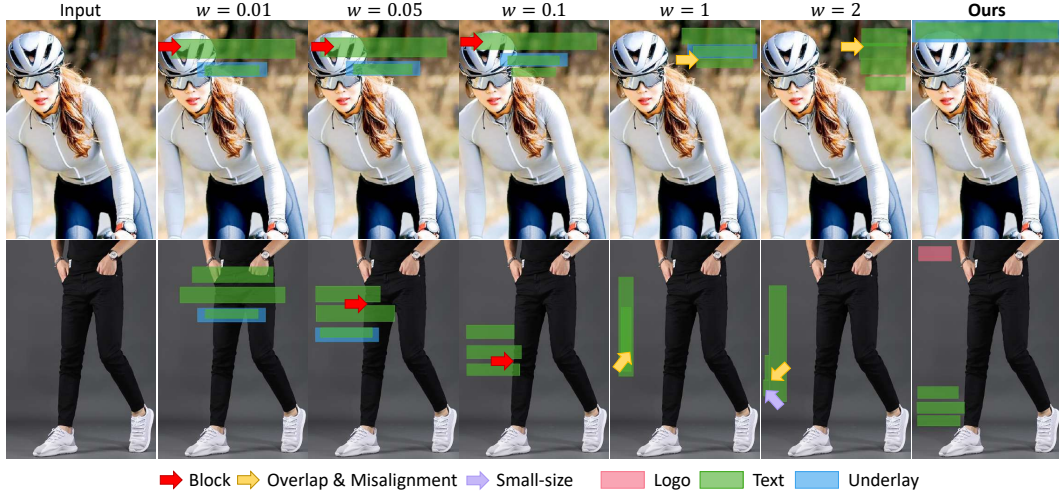


Figure 3: Exploration of the weight w on PKU dataset.

Based on the analysis above, we argue that the layout of generative space affects the balance between content and graphics. Therefore, we propose the content and graphic balance weight, denoted as ω . This weight is used to regulate the interaction between layout representations and image embeddings, optimizing the generation space. The arrangement of layout elements is inappropriate when ω is a constant, as shown in Fig. 3; more experiments are provided in Appendix C.2.

We first use a ViT-based [10] image encoder E_I for image embedding extraction. Then, we employ a trainable query transformer [28] network, which takes learnable query embeddings and image embeddings as input to predict ω . The weight ω is then mapped to the intermediate layers of the transformers via cross-attention:

$$\text{CrossAttention}(Q, K, V) = \text{softmax}\left(\frac{QK^T}{\sqrt{d}}\right) \cdot V. \quad (6)$$

Then we obtain the output X'' from the second group as follows:

$$X'' = X' + \omega * \text{CrossAttention}\left(W_Q \cdot X', W_K \cdot E_I(I \oplus S), W_V \cdot E_I(I \oplus S)\right). \quad (7)$$

Here, W_Q, W_K, W_V are learnable projection matrices, X' denotes a flattened intermediate representation of the first group of the layout decoder transformer block and \oplus represents concatenation. We found that this approach allows the model to achieve a good trade-off between graphic metrics and content-aware metrics, thereby enhancing performance in both areas.

3.4 Saliency Bounding Box

We found that the model’s alignment of geometric features between the layout representations and image embeddings is insufficient, likely due to the difference in modalities, with images in the visual domain and layouts in the geometric parameter domain. Furthermore, we noted that the saliency map effectively retains the key shapes of the canvas while removing other irrelevant high-frequency

details. Consequently, we employed a contour detection algorithm mentioned in Sec. 3.1 to process the saliency map, thereby obtaining saliency bounding box. The bounding box is encoded using the bounding encoder E_B implemented with a multi-layer perceptron (MLP). This step explicitly extracts the spatial information of salient regions in images and transforms it into data of the same modality as the layout elements, thus providing a more precise basis for the alignment of geometric features.

Similar to Sec. 3.3, we employ cross-attention to inject spatial information. Then we can get the output X''' of the third group of the transformer block as follows:

$$X''' = X'' + \text{CrossAttention} \left(W_Q' \cdot X'', W_K' \cdot E_B(B), W_V' \cdot E_B(B) \right), \quad (8)$$

where W_Q' , W_K' and W_V' are learnable projection matrices, X'' is the output of the second group of the layout decoder transformer block.

Since each saliency map contains only a few bounding boxes, the aforementioned process introduces only a minimal computational overhead while improving content and graphic performance.

4 Experiments

4.1 Datasets



Figure 4: Qualitative comparison of unconstrained generation on PKU and CGL.

We evaluated our method and state-of-the-art methods on two publicly available datasets: CGL [47] and PKU [17], obtained from e-commerce platforms, cover products like clothing, food and furniture.

The PKU dataset comprises 9,974 training and 905 test images containing layout elements such as logos, text, and underlays. The CGL dataset includes 60,548 image-layout pairs and 1,000 canvases. Appendix. A.1 provides additional details on data processing.

Since both datasets lack annotated validation and test sets, we followed the setup proposed by RALF [16], splitting the original training sets with a train/val/test ratio of roughly 8:1:1. This allowed us to conduct constrained generation tasks using ground truth labels. For comprehensive evaluation, we tested and compared all methods on both annotated and unannotated test sets.

4.2 Evaluation Metrics

Following previous works [17, 47], we evaluate primarily from the following two dimensions.

Graphic metrics. This part of the assessment focuses on measuring the graphic quality of the layout without considering the canvas. Underlay effectiveness (Und^\uparrow) describes whether the underlay element fully encompasses other elements. Und_L computes the overlap ratio between all non-underlay elements and the underlay element, selecting the maximum value. Und_S imposes stricter conditions, only including instances where the overlap ratio is 1. The Und metric is closely and positively linked with the quality of the layout. Overlay (Ove^\downarrow) represents the average IoU of all pairs of elements except for underlay elements, which is indicative of the layout’s neatness and organization.

Content-aware metrics. This part primarily evaluates the harmony between the layout and the canvas and measures the model’s content-awareness. Occlusion (Occ^\downarrow) calculates the average proportion of layout elements covering the saliency regions, identified through saliency maps. Readability (Rea^\downarrow) assesses the non-flatness of regions containing plain text elements without underlay decoration by calculating the average gradient of pixels in the layout area within the image space.

4.3 Implementation Details

Benefiting from the contributions made by RALF [16] in this field, we conducted fair comparisons based on multiple baseline re-implementations by the RALF team. Our model was trained for 500 epochs, using a batch size of 32 on PKU with a learning rate of 1e-4 and a batch size of 128 on CGL with a learning rate of 2e-4. We set the diffusion steps to 1000 and DDIM [35] sampling steps to 100. We use the Adam optimizer with $\beta_1 = 0.9$ and $\beta_2 = 0.999$, along with a cosine annealing learning rate scheduler. Specific details of the network architecture can be found in the Appendix. A.2.

4.4 Unconstrained Generation

Qualitative Comparison. Fig. 4 presents the qualitative results on the PKU and CGL datasets, respectively. The results demonstrate that our method is capable of addressing issues related to blocking, overlap, and misalignment. In contrast, the baseline methods often produce small-sized elements, overlapped text and logo elements, misaligned layouts between underlay and text, and unfit arrangements between layout and objects.

Table 1: Comparison of unconstrained generation methods on PKU and CGL annotated datasets.

Method	Params	PKU annotated					CGL annotated				
		Content		Graphic			Content		Graphic		
		Occ^\downarrow	Rea^\downarrow	Und_L^\uparrow	Und_S^\uparrow	Ove^\downarrow	Occ^\downarrow	Rea^\downarrow	Und_L^\uparrow	Und_S^\uparrow	Ove^\downarrow
CGL-GAN[47]	41M	0.176	0.0167	0.745	0.333	0.1071	0.196	0.0249	0.729	0.310	0.2574
DS-GAN[17]	30M	0.159	0.0161	0.828	0.295	0.0353	0.153	0.0198	0.886	0.545	0.0415
ICVT[4]	50M	0.280	0.0205	0.446	0.295	0.3155	0.227	0.0267	0.518	0.345	0.2337
LayoutDM [†] [19]	43M	0.151	0.0161	0.672	0.260	0.3224	0.152	0.0168	0.892	0.778	0.0325
RALF[16]	43M	0.138	0.0126	0.977	0.907	0.0069	0.140	0.0141	0.994	0.980	0.0046
CGB-DM(Ours)	48M	0.108	0.0120	0.999	0.988	0.0016	0.120	0.0156	0.998	0.990	0.0012

Quantitative Comparison. We present the quantitative comparison on the annotated datasets without constraints in Tab. 1. Our method achieves the best results overall, except for the Rea metric of RALF on CGL. Compared to other baselines, our approach performs exceptionally well on the Und and Ove metrics, approaching the performance achievable with ground truth labels. In summary, the results indicate that our method can perform well in both content metrics and graphic metrics.

Train	Test	Method	Occ ↓	Rea ↓	Und _L ↑	Unds ↑	Ove ↓
CGL	PKU-unanno	RALF	0.143	0.0170	0.989	0.958	0.0347
		Ours	0.110	0.0195	0.997	0.984	0.0017
PKU	PKU-anno	RALF	0.140	0.0113	0.995	0.976	0.0078
		Ours	0.112	0.0149	0.997	0.989	0.0025
CGL	CGL-unanno	RALF	0.342	0.0425	0.927	0.773	0.0309
		Ours	0.334	0.0350	0.999	0.984	0.0051
PKU	CGL-anno	RALF	0.150	0.0170	0.974	0.902	0.0065
		Ours	0.115	0.0134	0.995	0.975	0.0047

Table 2: Cross-evaluation setup: We train a model on PKU and test it on CGL, or vice versa.

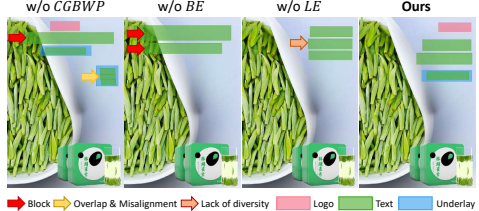


Figure 5: Ablation study of the contribution of each module on PKU dataset.

Out-of-domain generalization. To further validate the generalization and robustness of our method, we implemented a cross-evaluation setup. We train a model on PKU and then test it on CGL or vice versa. Tab. 2 summarizes our results. Notably, although RALF performed well, our method outperformed it in most metrics. The findings demonstrate our approach adapts well to diverse real-world background images, showcasing strong generalization capabilities.

4.5 Constrained Generation



Figure 6: Constrained qualitative comparison on PKU. Examples of input constraints and generated results for each constrained generation task. Quotation marks indicate the constraints.

Table 3: Comparison of constrained generation methods on PKU and CGL annotated datasets.

Method	PKU annotated					CGL annotated				
	Content		Graphic			Content		Graphic		
	Occ ↓	Rea ↓	Und _L ↑	Unds ↑	Ove ↓	Occ ↓	Rea ↓	Und _L ↑	Unds ↑	Ove ↓
C → S + P										
LayoutDM [†]	0.161	0.0171	0.669	0.274	0.2949	0.141	0.0150	0.924	0.830	0.0332
RALF	0.136	0.0127	0.967	0.890	0.0091	0.140	0.0142	0.987	0.969	0.0056
CGB-DM(Ours)	0.117	0.0131	0.986	0.947	0.0025	0.121	0.0141	0.992	0.970	0.0093
C + S → P										
LayoutDM [†]	0.162	0.0152	0.755	0.563	0.2063	0.142	0.0149	0.922	0.834	0.0268
RALF	0.138	0.0123	0.945	0.876	0.0113	0.143	0.0148	0.984	0.957	0.0051
CGB-DM(Ours)	0.123	0.0130	0.986	0.929	0.0093	0.138	0.0131	0.982	0.917	0.0035
Completion										
LayoutDM [†]	0.141	0.0148	0.549	0.235	0.1822	0.142	0.0149	0.877	0.757	0.0247
RALF	0.137	0.0132	0.970	0.905	0.0139	0.141	0.0144	0.988	0.966	0.0042
CGB-DM(Ours)	0.112	0.0122	0.991	0.968	0.0038	0.123	0.0142	0.978	0.944	0.0037
Refinement										
LayoutDM [†]	0.129	0.0112	0.910	0.599	0.0054	0.143	0.0145	0.890	0.614	0.0036
RALF	0.128	0.0103	0.989	0.951	0.0047	0.142	0.0136	0.994	0.980	0.0024
CGB-DM(Ours)	0.126	0.0101	0.991	0.967	0.0014	0.140	0.0134	0.989	0.946	0.0022

Designing constrained experiments allows us to tailor generated outputs to meet specific needs under various conditions. Following the framework established for content-agnostic generation [20], we assess various approaches across constrained tasks within content-aware generation.

Category → Size + Position ($C \rightarrow S + P$) means we specify the type of layouts, and the model generates the appropriate sizes and positions for each layout.

Table 4: Ablation on PKU and CGL annotated datasets.

Setting	PKU annotated					CGL annotated				
	Occ↓	Rea↓	Und _L ↑	Und _S ↑	Ove↓	Occ↓	Rea↓	Und _L ↑	Und _S ↑	Ove↓
Arch Selection										
W/O CGBWP	0.121	0.0151	0.999	0.991	0.0033	0.126	0.0168	0.998	0.990	0.0026
W/O BE	0.121	0.0142	0.992	0.974	0.0027	0.128	0.0166	0.997	0.985	0.0028
W/O LE	0.115	0.0151	0.998	0.979	0.0015	0.123	0.0168	0.998	0.987	0.0014
CGBWP Impact										
Image & Box	0.117	0.0140	0.997	0.983	0.0018	0.121	0.0160	0.998	0.989	0.0023
Box Only	0.111	0.0147	0.999	0.995	0.0010	0.121	0.0159	0.999	0.988	0.0027
Ours	0.108	0.0120	0.999	0.988	0.0016	0.120	0.0156	0.998	0.990	0.0012

Category + Size → Position(C + S → P) involves providing the types and sizes of layout elements as input and generating the position of each element accordingly.

Completion fixes the size and position for certain elements and generates a complete layout.

Refinement aims to correct layouts that have been perturbed with Gaussian noise, with a mean of 0 and a variance of 0.01, added to the true label values following [33].

Compared to other baselines that use constraint encoder, our method does not require additional modules. Specifically, we only need to treat the polluted data as an intermediate state in the reverse process for the refinement task, eliminating the need for additional training. For other tasks, we train and infer the corresponding constraint conditions in the form of masks.

The generated examples are shown in Fig. 6. Additionally, the content and graphic metrics are reported in Tab. 3. These results show that our method is effective for constrained tasks as well, achieving strong performance without an additional constraint encoder.

4.6 Ablation Study

We conducted extensive ablation studies to validate the proposed Layout Encoder(LE), CGBWP and Bounding Encoder(BE). To further explore the settings of weight ω , we performed weight ω ablation studies. And the related results are summarized in Tab. 4. All evaluations were performed on the PKU annotated dataset and CGL annotated dataset. The first row illustrates the shortcomings of solely using a constant weight ω without the CGBWP module. Further exploration in the fourth and fifth rows underscores the effectiveness of maintaining content and graphic balance, only incorporating *omega* from the CGBWP for the image. We find that there are still a few advantages in graphic metrics on PKU annotated when ω to saliency bounding box. The second row demonstrates that employing saliency bounding boxes can mitigate modality differences, resulting in improvements in both content and graphic metrics. The third row illustrates the importance of the LE module, especially in content metrics. We provide specific examples in Fig. 5 to show the function of each module. The Appendix. C.2 also provides ablation results on the PKU and CGL unannotated datasets.

5 Conclusion

In this paper, we introduce a method called the Content and Graphic Balance Transformer-based Diffusion Model (CGB-DM) to tackle content-aware layout generation tasks. This approach addresses key challenges in previous work, including overlap, misalignment, small-sized elements, and inadequate content-aware issues that can be summarized as content and graphic imbalance. We find that our method can focus on both content-aware features of images and graphic-aware features of layouts, achieving an optimal balance, due to the powerful generative and modeling capability of the transformer-based diffusion model. Furthermore, we design a regulator to adjust the interaction process between the layout representations and image embeddings, thereby optimizing the layout generation space. This space critically affects the balance between content and graphic elements. Additionally, we add the saliency bounding box to enhance the capability of capturing geometric information from the images. We conduct extensive experiments which demonstrate that our method outperforms all existing methods in both quantitative and qualitative performances. Our approach has the potential to be applicable to other graphic design fields.

References

- [1] Diego Martin Arroyo, Janis Postels, and Federico Tombari. Variational transformer networks for layout generation. In *IEEE Conf. Comput. Vis. Pattern Recog.*, 2021.
- [2] Jacob Austin, Daniel D Johnson, Jonathan Ho, Daniel Tarlow, and Rianne Van Den Berg. Structured denoising diffusion models in discrete state-spaces. In *Adv. Neural Inform. Process. Syst.*, 2021.
- [3] Tim Brooks, Bill Peebles, Connor Holmes, Will DePue, Yufei Guo, Li Jing, David Schnurr, Joe Taylor, Troy Luhman, Eric Luhman, Clarence Ng, Ricky Wang, and Aditya Ramesh. Video generation models as world simulators, 2024.
- [4] Yunning Cao, Ye Ma, Min Zhou, Chuanbin Liu, Hongtao Xie, Tiezheng Ge, and Yuning Jiang. Geometry aligned variational transformer for image-conditioned layout generation. In *ACM Int. Conf. Multimedia*, 2022.
- [5] Shang Chai, Liansheng Zhuang, and Fengying Yan. Layoutdm: Transformer-based diffusion model for layout generation. In *IEEE Conf. Comput. Vis. Pattern Recog.*, 2023.
- [6] Jian Chen, Ruiyi Zhang, Yufan Zhou, and Changyou Chen. Towards aligned layout generation via diffusion model with aesthetic constraints. *arXiv preprint arXiv:2402.04754*, 2024.
- [7] Junsong Chen, Jincheng Yu, Chongjian Ge, Lewei Yao, Enze Xie, Yue Wu, Zhongdao Wang, James Kwok, Ping Luo, Huchuan Lu, et al. Pixart-alpha: Fast training of diffusion transformer for photorealistic text-to-image synthesis. *arXiv preprint arXiv:2310.00426*, 2023.
- [8] Chin-Yi Cheng, Forrest Huang, Gang Li, and Yang Li. Play: Parametrically conditioned layout generation using latent diffusion. *arXiv preprint arXiv:2301.11529*, 2023.
- [9] Biplab Deka, Zifeng Huang, Chad Franzen, Joshua Hibschnan, Daniel Afergan, Yang Li, Jeffrey Nichols, and Ranjitha Kumar. Rico: A mobile app dataset for building data-driven design applications. In *ACM Sym. User Inter. Soft. Tech.*, 2017.
- [10] Alexey Dosovitskiy, Lucas Beyer, Alexander Kolesnikov, Dirk Weissenborn, Xiaohua Zhai, Thomas Unterthiner, Mostafa Dehghani, Matthias Minderer, Georg Heigold, Sylvain Gelly, et al. An image is worth 16x16 words: Transformers for image recognition at scale. *arXiv preprint arXiv:2010.11929*, 2020.
- [11] Patrick Esser, Sumith Kulal, Andreas Blattmann, Rahim Entezari, Jonas Müller, Harry Saini, Yam Levi, Dominik Lorenz, Axel Sauer, Frederic Boesel, et al. Scaling rectified flow transformers for high-resolution image synthesis. *arXiv preprint arXiv:2403.03206*, 2024.
- [12] Ian Goodfellow, Jean Pouget-Abadie, Mehdi Mirza, Bing Xu, David Warde-Farley, Sherjil Ozair, Aaron Courville, and Yoshua Bengio. Generative adversarial networks. *Communications ACM*, 63(11):139–144, 2020.
- [13] Shunan Guo, Zhuochen Jin, Fuling Sun, Jingwen Li, Zhaorui Li, Yang Shi, and Nan Cao. Vinci: an intelligent graphic design system for generating advertising posters. In *CHI Conf. Human. In Comput. Sys.*, 2021.
- [14] Kamal Gupta, Justin Lazarow, Alessandro Achille, Larry S Davis, Vijay Mahadevan, and Abhinav Shrivastava. Layouttransformer: Layout generation and completion with self-attention. In *Int. Conf. Comput. Vis.*, 2021.
- [15] Jonathan Ho, Ajay Jain, and Pieter Abbeel. Denoising diffusion probabilistic models. In *Adv. Neural Inform. Process. Syst.*, 2020.
- [16] Daichi Horita, Naoto Inoue, Kotaro Kikuchi, Kota Yamaguchi, and Kiyoharu Aizawa. Retrieval-augmented layout transformer for content-aware layout generation. In *IEEE Conf. Comput. Vis. Pattern Recog.*, 2023.
- [17] Hsiao Yuan Hsu, Xiangteng He, Yuxin Peng, Hao Kong, and Qing Zhang. Posterlayout: A new benchmark and approach for content-aware visual-textual presentation layout. In *IEEE Conf. Comput. Vis. Pattern Recog.*, 2023.

[18] Mude Hui, Zhizheng Zhang, Xiaoyi Zhang, Wenxuan Xie, Yuwang Wang, and Yan Lu. Unifying layout generation with a decoupled diffusion model. In *IEEE Conf. Comput. Vis. Pattern Recog.*, 2023.

[19] Naoto Inoue, Kotaro Kikuchi, Edgar Simo-Serra, Mayu Otani, and Kota Yamaguchi. Layoutdm: Discrete diffusion model for controllable layout generation. In *Int. Conf. Comput. Vis.*, 2023.

[20] Zhaoyun Jiang, Jiaqi Guo, Shizhao Sun, Huayu Deng, Zhongkai Wu, Vuksan Mijovic, Zijiang James Yang, Jian-Guang Lou, and Dongmei Zhang. Layoutformer++: Conditional graphic layout generation via constraint serialization and decoding space restriction. In *IEEE Conf. Comput. Vis. Pattern Recog.*, 2023.

[21] Zhaoyun Jiang, Shizhao Sun, Jihua Zhu, Jian-Guang Lou, and Dongmei Zhang. Coarse-to-fine generative modeling for graphic layouts. In *Assoc. Adv. Artif. Intell.*, 2022.

[22] Kotaro Kikuchi, Edgar Simo-Serra, Mayu Otani, and Kota Yamaguchi. Constrained graphic layout generation via latent optimization. In *ACM Int. Conf. Multimedia*, 2021.

[23] Xiang Kong, Lu Jiang, Huiwen Chang, Han Zhang, Yuan Hao, Haifeng Gong, and Irfan Essa. Blt: Bidirectional layout transformer for controllable layout generation. In *Eur. Conf. Comput. Vis.*, 2022.

[24] Hsin-Ying Lee, Lu Jiang, Irfan Essa, Phuong B Le, Haifeng Gong, Ming-Hsuan Yang, and Weilong Yang. Neural design network: Graphic layout generation with constraints. In *Eur. Conf. Comput. Vis.*, 2020.

[25] Elad Levi, Eli Brosh, Mykola Mykhailych, and Meir Perez. Dlt: Conditioned layout generation with joint discrete-continuous diffusion layout transformer. In *Int. Conf. Comput. Vis.*, 2023.

[26] Fengheng Li, An Liu, Wei Feng, Honghe Zhu, Yaoyu Li, Zheng Zhang, Jingjing Lv, Xin Zhu, Junjie Shen, Zhangang Lin, et al. Relation-aware diffusion model for controllable poster layout generation. In *ACM Int. Conf. Multimedia*, 2023.

[27] Jianan Li, Jimei Yang, Aaron Hertzmann, Jianming Zhang, and Tingfa Xu. Layoutgan: Generating graphic layouts with wireframe discriminators. *arXiv preprint arXiv:1901.06767*, 2019.

[28] Junnan Li, Dongxu Li, Silvio Savarese, and Steven Hoi. Blip-2: Bootstrapping language-image pre-training with frozen image encoders and large language models. In *Int. Conf. Mach. Learn.*, 2023.

[29] Peter O’Donovan, Aseem Agarwala, and Aaron Hertzmann. Designscape: Design with interactive layout suggestions. In *ACM Conf. Human Factors Comput. Sys.*, 2015.

[30] Akshay Gadi Patil, Omri Ben-Eliezer, Or Perel, and Hadar Averbuch-Elor. Read: Recursive autoencoders for document layout generation. In *IEEE Conf. Comput. Vis. Pattern Recog. Worksh.*, 2020.

[31] William Peebles and Saining Xie. Scalable diffusion models with transformers. In *Int. Conf. Comput. Vis.*, 2023.

[32] Xuebin Qin, Hang Dai, Xiaobin Hu, Deng-Ping Fan, Ling Shao, and Luc Van Gool. Highly accurate dichotomous image segmentation. In *Eur. Conf. Comput. Vis.*, 2022.

[33] Soliha Rahman, Vinoth Pandian Sermuga Pandian, and Matthias Jarke. Ruite: Refining ui layout aesthetics using transformer encoder. In *Int. Conf. Intel. User. Interfaces-Companion*, 2021.

[34] Robin Rombach, Andreas Blattmann, Dominik Lorenz, Patrick Esser, and Björn Ommer. High-resolution image synthesis with latent diffusion models. In *IEEE Conf. Comput. Vis. Pattern Recog.*, pages 10684–10695, 2022.

[35] Jiaming Song, Chenlin Meng, and Stefano Ermon. Denoising diffusion implicit models. *arXiv preprint arXiv:2010.02502*, 2020.

[36] Roman Suvorov, Elizaveta Logacheva, Anton Mashikhin, Anastasia Remizova, Arsenii Ashukha, Aleksei Silvestrov, Naejin Kong, Harshith Goka, Kiwoong Park, and Victor Lempitsky. Resolution-robust large mask inpainting with fourier convolutions. In *IEEE Winter Conf. Appl. Comput. Vis.*, 2022.

[37] Zecheng Tang, Chenfei Wu, Juntao Li, and Nan Duan. Layoutnuwa: Revealing the hidden layout expertise of large language models. *arXiv preprint arXiv:2309.09506*, 2023.

[38] Ashish Vaswani, Noam Shazeer, Niki Parmar, Jakob Uszkoreit, Llion Jones, Aidan N Gomez, Łukasz Kaiser, and Illia Polosukhin. Attention is all you need. In *Adv. Neural Inform. Process. Syst.*, 2017.

[39] Bo Wang, Quan Chen, Min Zhou, Zhiqiang Zhang, Xiaogang Jin, and Kun Gai. Progressive feature polishing network for salient object detection. In *Assoc. Adv. Artif. Intell.*, 2020.

[40] Weihao Xia, Yulun Zhang, Yujiu Yang, Jing-Hao Xue, Bolei Zhou, and Ming-Hsuan Yang. Gan inversion: A survey. *IEEE Trans. Pattern Anal. Mach. Intell.*, 45(3):3121–3138, 2022.

[41] Chenchen Xu, Min Zhou, Tiezheng Ge, Yuning Jiang, and Weiwei Xu. Unsupervised domain adaption with pixel-level discriminator for image-aware layout generation. In *IEEE Conf. Comput. Vis. Pattern Recog.*, 2023.

[42] Xuyong Yang, Tao Mei, Ying-Qing Xu, Yong Rui, and Shipeng Li. Automatic generation of visual-textual presentation layout. *ACM Trans. Multimedia Comput. Commun. App.*, 2016.

[43] Junyi Zhang, Jiaqi Guo, Shizhao Sun, Jian-Guang Lou, and Dongmei Zhang. Layoutdiffusion: Improving graphic layout generation by discrete diffusion probabilistic models. In *Int. Conf. Comput. Vis.*, 2023.

[44] Peiying Zhang, Chenhui Li, and Changbo Wang. Smarttext: Learning to generate harmonious textual layout over natural image. In *Int. Conf. Multimedia and Expo*, 2020.

[45] Xinru Zheng, Xiaotian Qiao, Ying Cao, and Rynson WH Lau. Content-aware generative modeling of graphic design layouts. In *ACM Trans. Graph.*, 2019.

[46] Xu Zhong, Jianbin Tang, and Antonio Jimeno Yepes. Publaynet: largest dataset ever for document layout analysis. In *Inter. Conf. Docu. Analy. Recog.*, 2019.

[47] Min Zhou, Chenchen Xu, Ye Ma, Tiezheng Ge, Yuning Jiang, and Weiwei Xu. Composition-aware graphic layout gan for visual-textual presentation designs. *arXiv preprint arXiv:2205.00303*, 2022.

Appendix

In this Appendix, we provide additional results and analysis.

Table of contents:

- Section A :Implementation Details
- Section B :More discussions
- Section C :Additional Experimental Results and Analysis

A Implementation Details

A.1 Data process

In the original datasets, PKU [17] provides inpainted images, while CGL [47] only offers images with authentic labels. Additionally, the quality of PKU’s inpainted images is not optimal, as they still retain traces of the original layout elements. We argue that this could adversely affect the model training process. Therefore, to ensure a fair comparison and obtain high-quality training data, we opted to use the inpainting algorithm [36] to enhance the repaired areas in both datasets.

While previous methods mainly relied on the PFPN [39] and BASNet [44] algorithms for saliency map extraction, the connectivity of PFPN’s weights has become defunct. Consequently, we have resorted to ISNet [32] and BASNet for reobtaining saliency maps. In line with previous methods, we combine the saliency maps obtained from both algorithms using a maximum operation.

In data partitioning, we adhere to the division criteria established by the RALF team to re-implement other methods. Similarly, we have excluded data with more than 11 elements from our training set at PKU.

A.2 Architecture details

We have provided all the details of the model in the Tab. 5.

Table 5: Network Parameters

module	layers	dim	FFN-dim	head
Layout Encoder	2	512	1024	8
Layout Decoder	4	512	1024	8
Image Encoder	6	512	2048	8
CGBWP(Q-former)	2	512	2048	8

Layout Encoder & Layout Decoder. Both the layout encoder and layout decoder consist of a series of transformer blocks. We use a two-layer transformer in the encoder and a four-layer transformer in the decoder. The key difference is that the layout decoder incorporates a cross-attention module to interact with the image embedding and saliency bounding box.

Image Encoder. We utilize ViT-like transformer blocks as our image encoder for effective visual feature extraction. We resized the input images to 384×256 to match the resolution of the original data, using a patch size of 32.

CGBWP. We employ a trainable query transformer network, as described in [28], to implement the CGBWP module. Unlike the Image Encoder, the Q-former network comprises only two layers. We utilize N learnable query embeddings as input, enabling interaction with image features through self-attention layers. The output activation function chosen is Softplus.

Bounding Encoder. We utilize a bounding encoder implemented with a three-layer MLP network to encode the salient bounding box, matching the dimensions required by the subsequent model. Specifically, the network’s input dimension is 4, while both the intermediate and output dimensions are 512. Softplus activation functions are used throughout.

A.3 Training details

All our experiments were conducted on NVIDIA 4090 GPU. For our proposed method, CGB-DM, we trained the model for 500 epochs on both PKU and CGL datasets. On PKU, the batch size was 32, the learning rate was 1e-4, and the training time was approximately 4 hours. On CGL, the batch size was 128, the learning rate was 2e-4, and the training time was around 10 hours.

Building upon the replication efforts of the RALF team, we retrained the benchmark methods—CGL-GAN, DS-GAN, ICVT, LayoutDM, and RALF—on the datasets we processed for comparison.

B More discussions

B.1 Limitations

We need to point out the limitations of this work: 1) Our layout encoder and decoder rely on the number of layout element categories, limiting our generated layouts to a finite set of categories and hindering their applicability to diverse real-world graphic design. Therefore, exploring open-vocabulary layout generation is necessary. 2) Our current approach primarily uses images as control conditions. We highlight that introducing additional constraints, such as text, is a promising direction for future research.

B.2 Potential societal impacts

Positive societal impacts of our CGB-DM include the ability to significantly enhance the efficiency and creativity of graphic design processes. By automating layout generation, designers can focus more on creative tasks, potentially leading to more innovative and visually appealing designs. However, as with other generative models, our CGB-DM could inadvertently create fake advertisements or magazine layouts, potentially leading to deception and the spread of misinformation.

C Additional Experimental Results and Analysis

We provided additional quantitative results and qualitative comparisons on both the PKU and CGL datasets.

Table 6: Comparison of unconstrained generation methods on PKU unannotated datasets.

Method	Params	PKU unannotated				
		Content		Graphic		
		Occ \downarrow	Rea \downarrow	Und \uparrow	Und \uparrow	Ove \downarrow
CGL-GAN[47]	41M	0.213	0.0256	0.718	0.299	0.1034
DS-GAN[17]	30M	0.179	0.0228	0.764	0.464	0.0368
ICVT[4]	50M	0.295	0.0254	0.420	0.301	0.3167
LayoutDM †[19]	43M	0.153	0.0220	0.645	0.235	0.3051
RALF[16]	43M	0.142	0.0190	0.965	0.878	0.0106
CGB-DM(Ours)	48M	0.117	0.0185	0.999	0.988	0.0018

C.1 Unconstrained generation on unannotated datasets

Tab. 6 demonstrates that even on the unannotated PKU dataset, our method achieves significant advantages. Specifically, regarding underlay effectiveness and overlap issues, our method performs comparably to its performance on the annotated dataset. In contrast, other baselines exhibit some degree of performance degradation. This indicates that CGB-DM can better overcome data differences and possesses superior generalization capabilities.

We also conducted similar comparative tests on the unannotated CGL dataset, with the summarized experimental results presented in Tab. 7. We observed that all methods show a decline in metrics when evaluated on the unannotated CGL dataset. Firstly, in terms of graphic metrics, other baseline

Table 7: Comparison of unconstrained generation methods on CGL unannotated datasets.

Method	Params	CGL unannotated					
		Content			Graphic		
		Uti↑	Occ↓	Rea↓	Und _L ↑	Und _S ↑	Ove↓
CGL-GAN[47]	41M	0.072	0.496	0.0604	0.652	0.129	0.2478
DS-GAN[17]	30M	0.131	0.407	0.0533	0.804	0.349	0.0831
ICVT[4]	50M	0.058	0.464	0.0502	0.466	0.306	0.1959
LayoutDM [†] [19]	43M	0.024	0.432	0.0499	0.730	0.539	0.0979
RALF[16]	43M	0.056	0.258	0.0319	0.986	0.935	0.0572
CGB-DM(Ours)	48M	0.104	0.346	0.0389	0.996	0.979	0.0041

Table 8: Ablation on PKU and CGL unannotated datasets.

Modules	PKU unannotated					CGL unannotated				
	Occ↓	Rea↓	Und _L ↑	Und _S ↑	Ove↓	Occ↓	Rea↓	Und _L ↑	Und _S ↑	Ove↓
Arch Selection										
W/O CGBWP	0.140	0.0199	0.999	0.994	0.0024	0.366	0.0417	0.995	0.991	0.0053
W/O BE	0.130	0.0194	0.995	0.969	0.0025	0.359	0.0391	0.994	0.961	0.0064
W/O LE	0.132	0.0202	0.999	0.979	0.0017	0.350	0.0403	0.993	0.972	0.0042
CGBWP Impact										
Image & Box	0.125	0.0193	0.998	0.985	0.0027	0.348	0.0384	0.996	0.982	0.0053
Box Only	0.132	0.0214	0.999	0.991	0.0026	0.358	0.0396	0.997	0.963	0.0044
Ours	0.117	0.0185	0.999	0.988	0.0018	0.346	0.0389	0.996	0.979	0.0041

methods exhibit a significant decline compared to the CGL annotated dataset. In contrast, our results demonstrate more robust performance. For instance, we achieve a score of 0.0041 on Ove, and obtain results of 0.996 and 0.979 on UndL and UndS, respectively. The results of other methods on Ove are generally greater than 0.05, which can significantly impact layout quality.

Furthermore, in content metrics, our method performs inferior to RALF but superior to other baselines. We need to elucidate the underlying reasons for this observation. As shown in Tab. 7, we introduced the Uti metric, which calculates the proportion of layout occupancy in non-significant regions. While Uti cannot serve as a reliable indicator of layout quality (since randomly generated cluttered layouts can also exhibit high Uti), a low Uti implies that the model struggles to generate layouts meeting basic requirements. The data in the table indicates that only our CGB-DM and DS-GAN achieve a Uti above 0.100, while RALF’s Uti is merely 0.056. Fig. 10 provides more intuitive insights. Thus, although RALF perform well in content metrics, its generated results exhibit serious content and graphic imbalance, resulting in lower layout quality due to its tendency to generate small-sized elements.

Finally, we explain from the perspective of layout constraints. The data distribution of the unannotated CGL dataset significantly differs from the training data, characterized by complex backgrounds or large significant regions in the images. This compresses the generation space, making it difficult for the model to find suitable layout generation positions. This also explains why other methods encounter content and graphic imbalance issues.

C.2 More results on ablation study

We also performed ablation studies on the unannotated PKU and CGL datasets. Tab. 8 summarizes the experimental results. Additionally, we provide further visual comparisons of the ablation experiments in Fig. 7 and Fig. 8.

C.3 Visual comparison

Fig. 9 and Fig. 11 provides additional qualitative comparisons on the PKU dataset without constraints. It is worth highlighting that Fig. 12 showcases the embellishment element, an extra category included

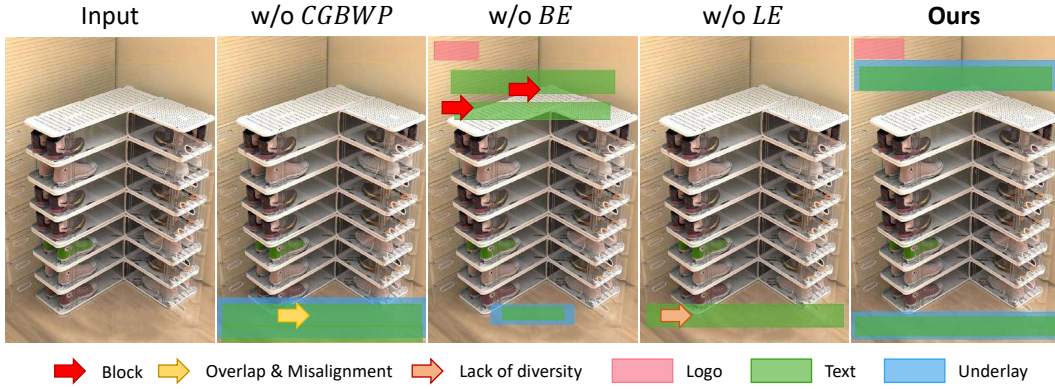


Figure 7: Ablation study of the contribution of each module on PKU dataset.

in the CGL dataset that serves to decorate and enhance the visual appeal. However, due to the sparse distribution of this category in the original dataset, we did not emphasize it in the main text.

The results intuitively demonstrate that other baselines struggle to consistently generate reasonable layouts when confronted with diverse background images, exhibiting issues such as overlap, misalignment, small-sized elements, and blocking.

Furthermore, in Fig. 13 and Fig. 14, we also present more results of constrained generation. The results indicate that even in constrained generation tasks, our method can generate high-quality layouts while strictly adhering to the given constraints without the need for an additional constraint encoder.

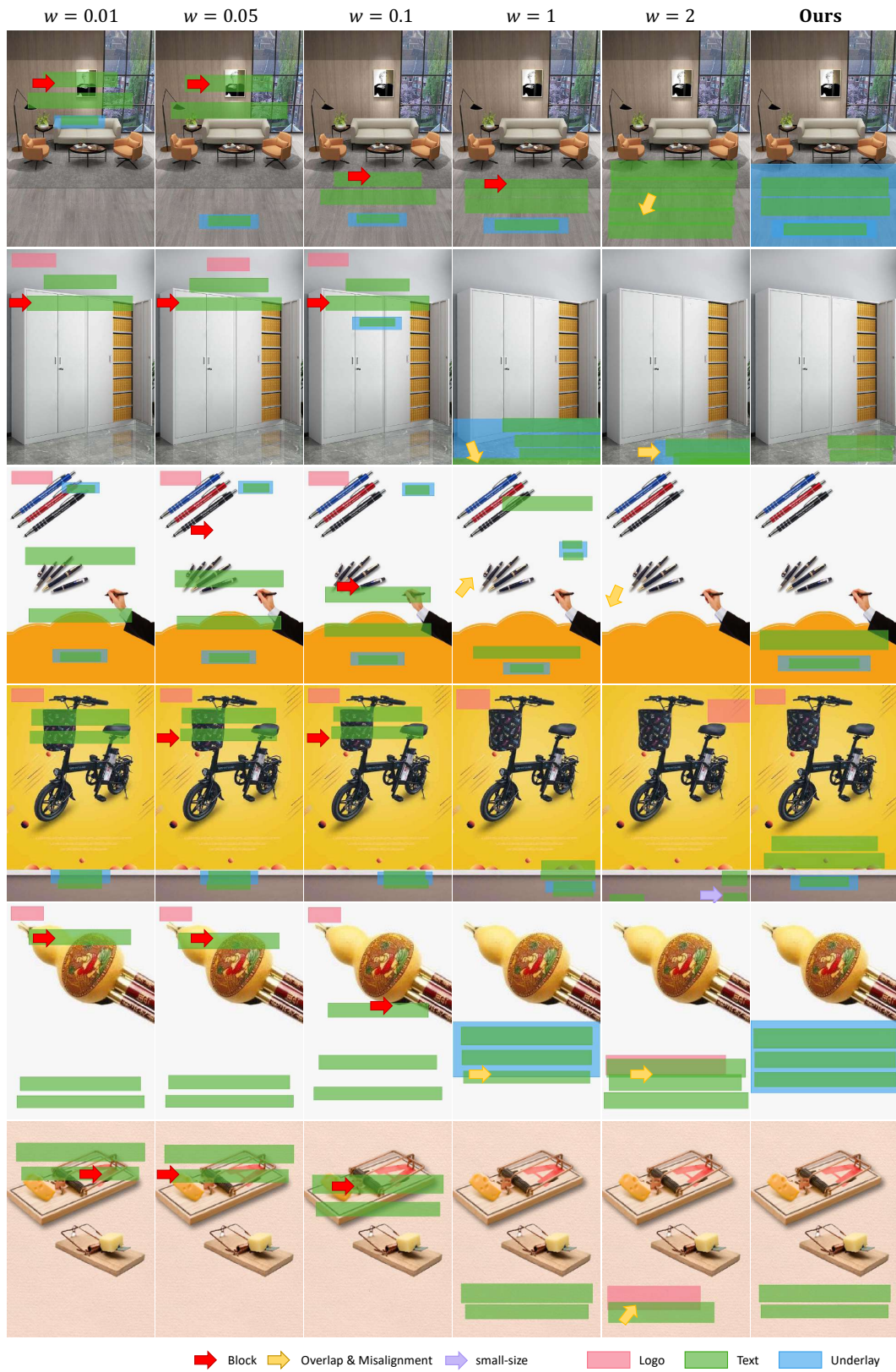


Figure 8: Ablation study of the weight ω on PKU dataset.

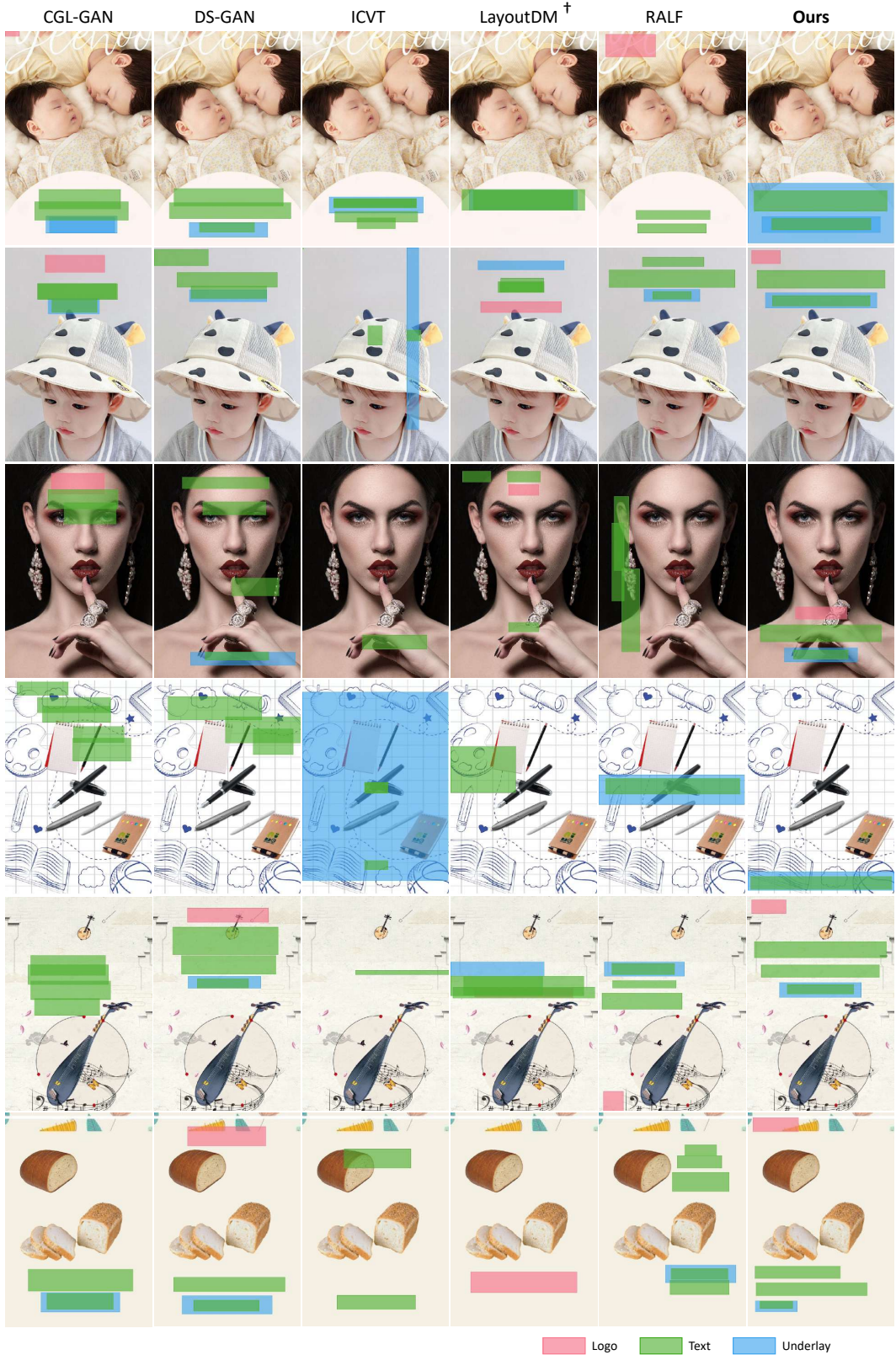


Figure 9: Qualitative comparison on PKU unannotated.

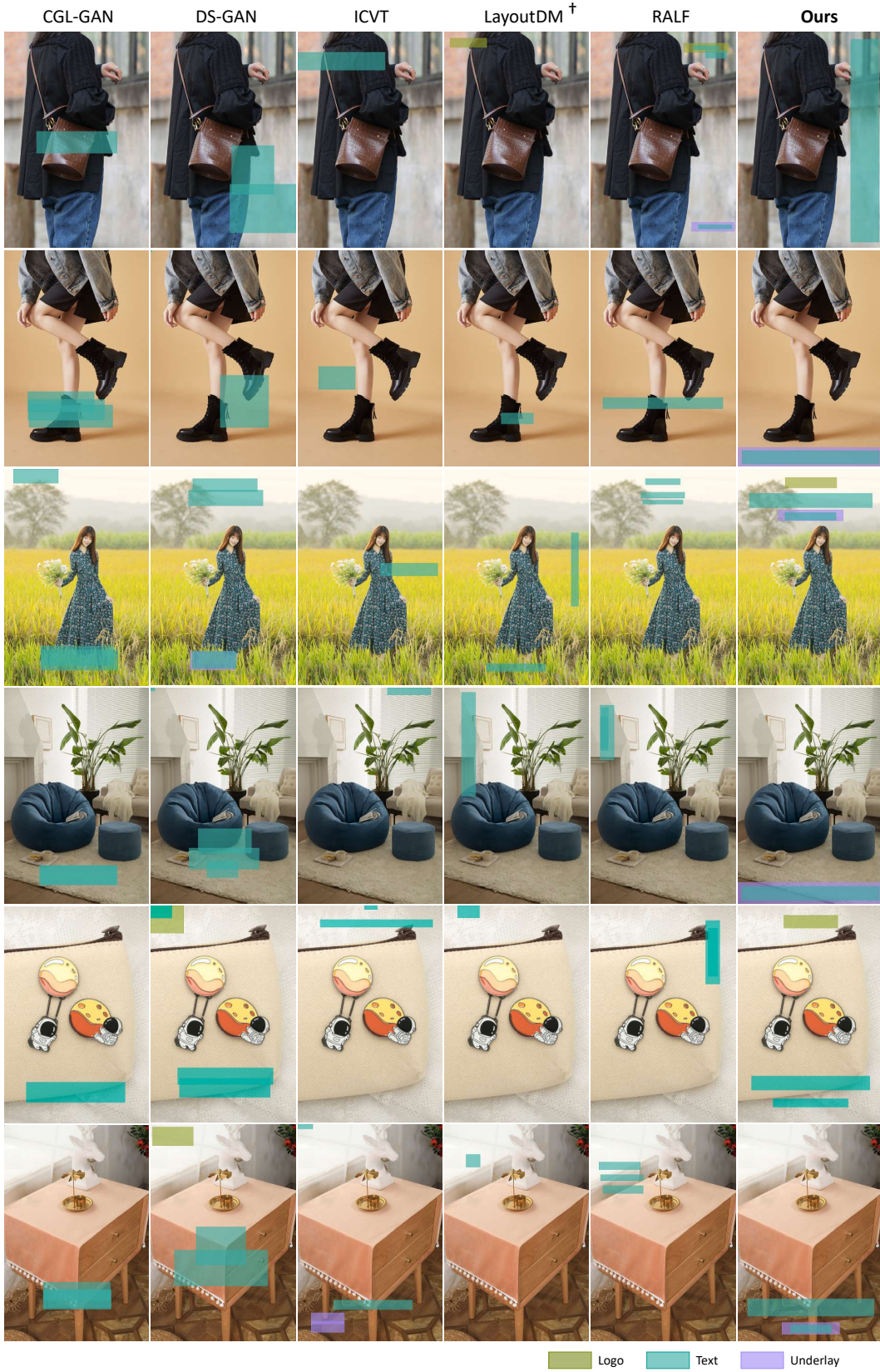


Figure 10: Qualitative comparison on CGL unannotated.

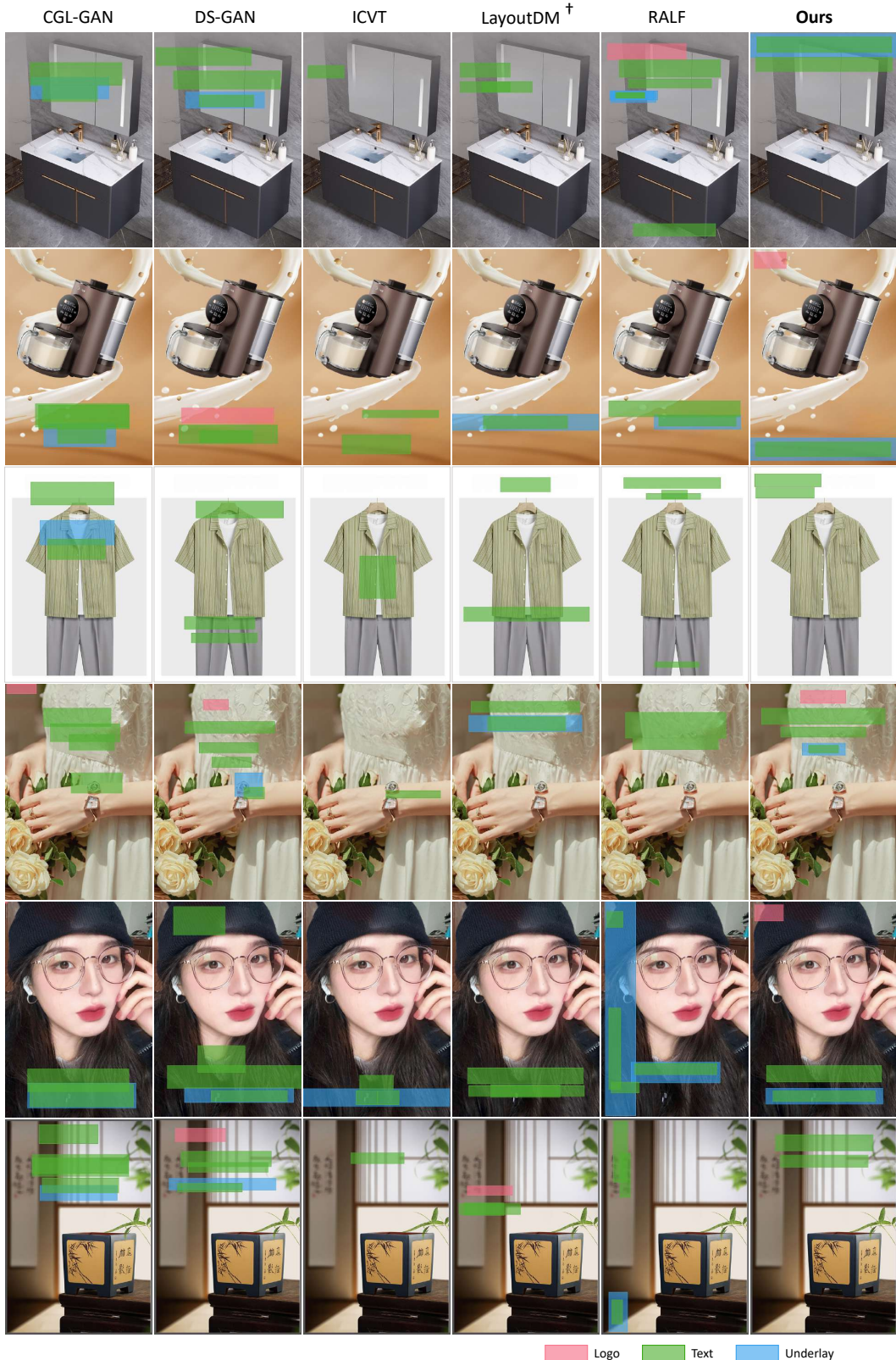


Figure 11: Qualitative comparison on PKU annotated.

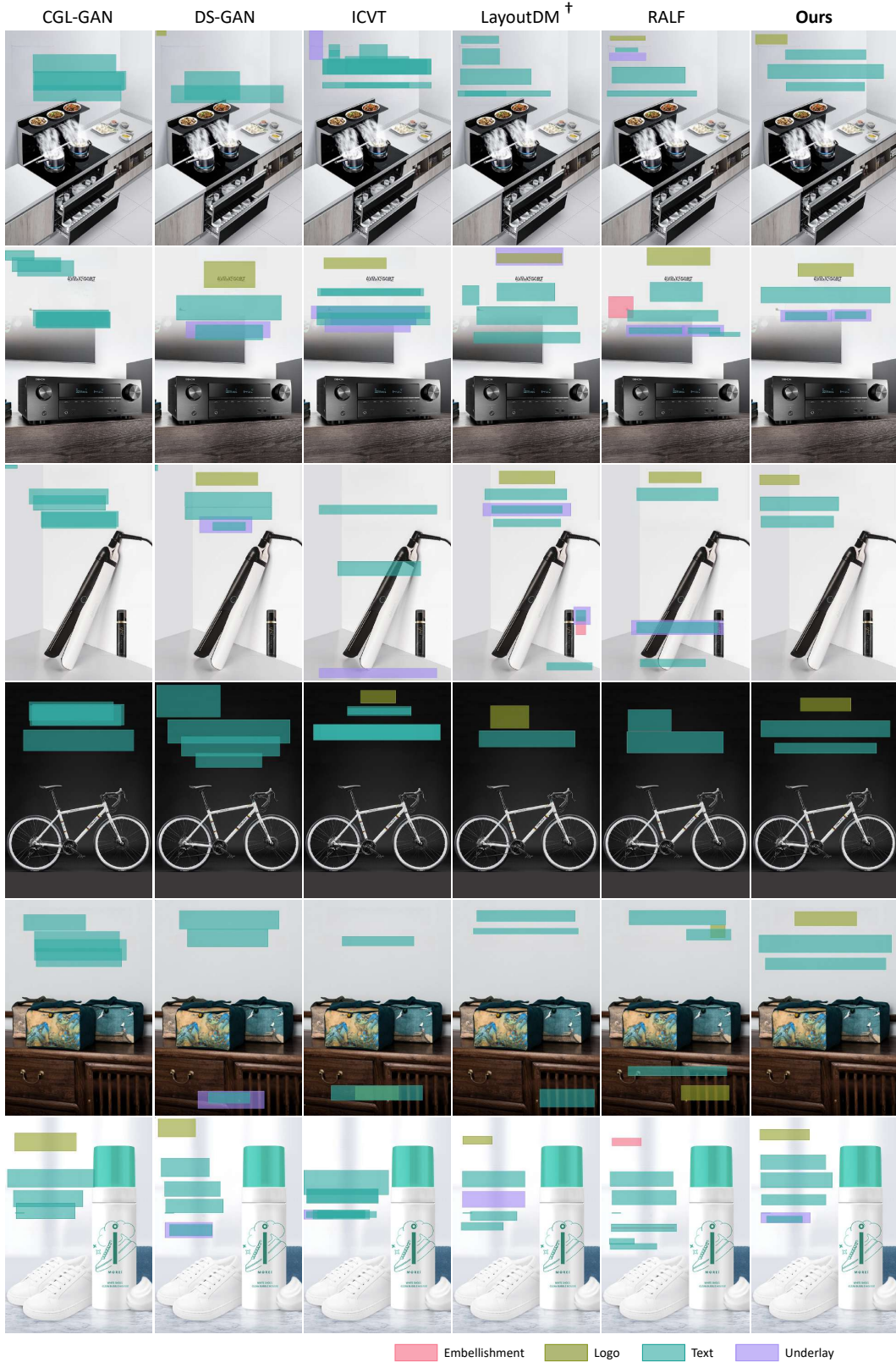


Figure 12: Qualitative comparison on CGL annotated.

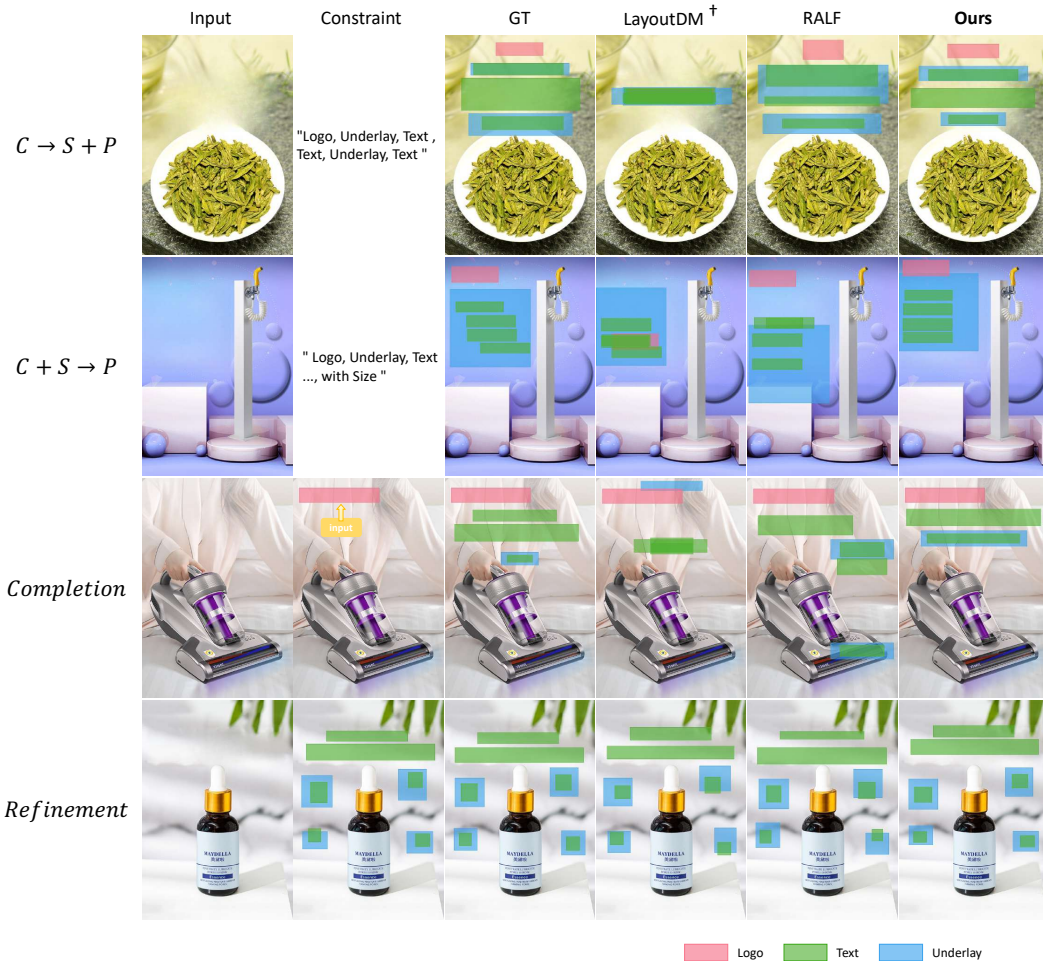


Figure 13: Constrained qualitative comparison on PKU annotated.

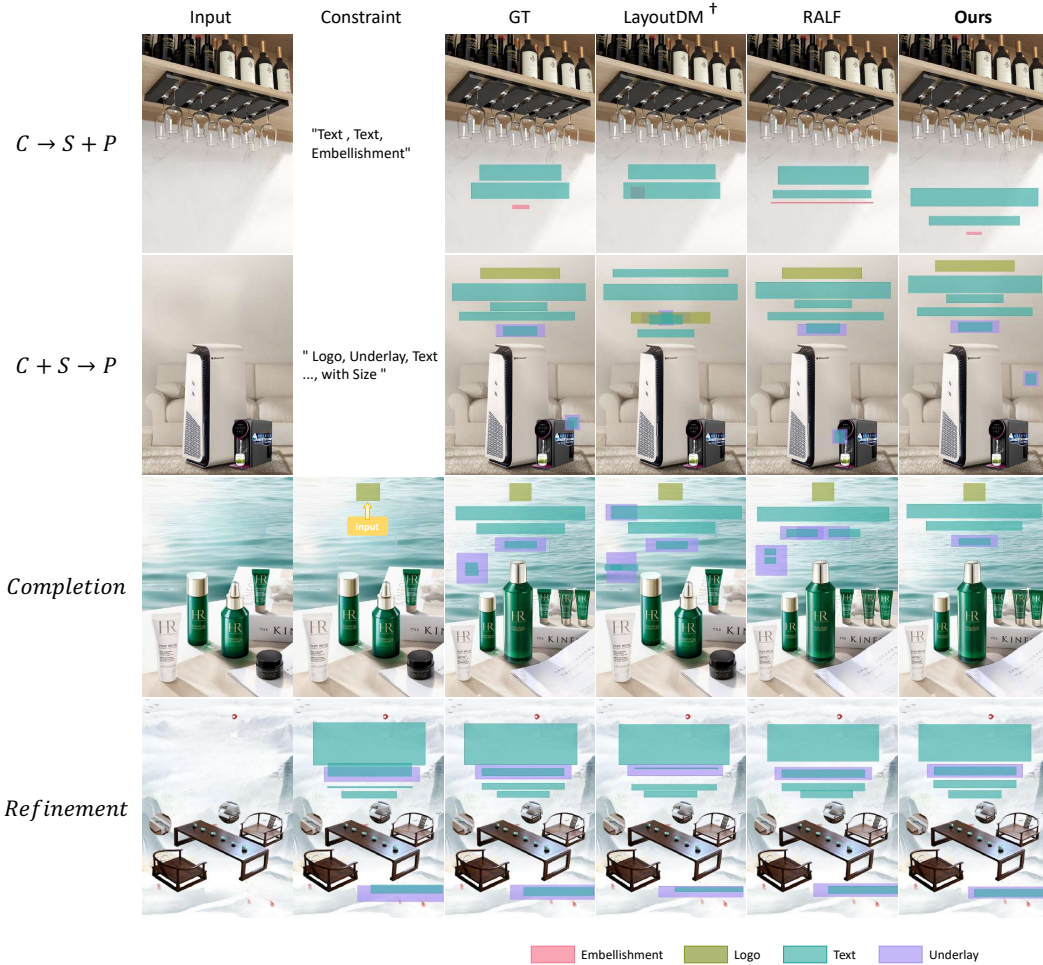


Figure 14: Constrained qualitative comparison on CGL annotated.